
TENGRAD: TIME-EFFICIENT NATURAL GRADIENT DESCENT WITH EXACT FISHER-BLOCK INVERSION

A PREPRINT

Saeed Soori

Department of Computer Science
University of Toronto
saeed.soori.sh@gmail.com

Bugra Can

Department of MSIS
Rutgers Business School
bugra.can@rutgers.edu

Baourun Mu

Department of Computer Science
University of Toronto
baorun.mu@mail.utoronto.ca

Mert Gürbüzbalaban

Department of MSIS
Rutgers Business School
mert.gurbuzbalaban@rutgers.edu

Maryam Mehri Dehnavi

Department of Computer Science
University of Toronto
mmehride@cs.toronto.edu

ABSTRACT

This work proposes a time-efficient Natural Gradient Descent method, called TENGraD, with linear convergence guarantees. Computing the inverse of the neural network’s Fisher information matrix is expensive in NGD because the Fisher matrix is large. Approximate NGD methods such as KFAC attempt to improve NGD’s running time and practical application by reducing the Fisher matrix inversion cost with approximation. However, the approximations do not reduce the overall time significantly and lead to less accurate parameter updates and loss of curvature information. TENGraD, improves the time efficiency of NGD by computing Fisher-block inverses with a computationally efficient covariance factorization and reuse method. It computes the inverse of each block exactly using the Woodbury matrix identity to preserve curvature information while admitting (linear) fast convergence rates. Our experiments on image classification tasks for state-of-the-art deep neural architecture on CIFAR-10, CIFAR-100, and Fashion-MNIST show that TENGraD significantly outperforms state-of-the-art NGD methods and often stochastic gradient descent in wall-clock time.

1 Introduction

Second order methods specifically Natural Gradient Descent (NGD) [1, 2, 3, 4] have gained traction in recent years as they accelerate the training of deep neural networks (DNN) by capturing the geometry of the optimization landscape [5] with the Fisher Information Matrix (FIM) [6, 4, 7]. NGD’s running time depends on both the convergence rate and computations per iteration which typically involves computing and inverting the FIM [8]. Exact NGD [9] methods demonstrate improved convergence compared to first order techniques such as Stochastic Gradient Descent (SGD)[10], and approximate NGD variants attempt to improve the time per iteration, hence the overall time, with approximation [8, 11, 12]. However, to our knowledge, none of the current approximate NGD approaches outperform or are comparable with the end-to-end wall-clock time of tuned SGD when training DNNs [8, 11, 12].

Exact NGD methods such as [9] and [13] improve the convergence of training DNNs compared to first-order methods, however, they are typically expensive and do not scale due to high computational complexity per iteration. The work in [13] derives an analytic formula for the linear network using the generalized inverse of the curvature which cannot be used for training state-of-the-art models due to lack of non-linear activation functions. Zhang *et al.* [9] extend NGD to deep nonlinear networks with non-smooth activations and show that NGD converges to the global optimum with a linear rate. However, their method fails to scale to large or even moderate size models primarily because it relies heavily on backpropagating Jacobian matrices, which scales with the network’s output dimension [14]. In [15] the authors use Woodbury identity for the inversion of Fisher matrix and propose a unified framework for subsampled Gauss-Newton

and NGD methods. Their framework is limited to fully connected networks and relies on empirical Fisher and requires extra forward-backward passes to perform parameter updates which slows down the training [16, 14].

Approximate NGD approaches such as [8, 11, 12, 17, 18, 19] attempt to improve the overall execution time of NGD with FIM inverse approximation, however, due to costly operations in the inverse approximation process they do not noticeably reduce the overall NGD time. In these methods, the FIM is approximated with a block-diagonal matrix, where blocks correspond to layers. The dimension of each block scales with the input and output dimension of the layer and therefore it cannot be computed and inverted efficiently for wide layers. To alleviate this cost, some methods further approximate each block inverse to reduce its size and computation complexity. For example, KFAC [8], approximates each block inverse using the Kronecker product of two smaller matrices, i.e. Kronecker factors. However, these factors have large sizes for wide layers and hence their inversion is expensive. EKfAC [11] improves the approximation used in KFAC by rescaling the Kronecker factors with a diagonal matrix obtained via costly singular value decompositions. Other work such as KBFGS [12] further estimates the inverse of Kronecker factors using low-rank BFGS types updates. WoodFisher [20] estimates the empirical FIM block inverses using rank-one updates, however, this estimation will not contain enough useful curvature information to produce a good search direction [21]. Our proposed method, TENGrAD, improves the time efficiency of NGD by reducing the FIM block inversion cost using a computationally efficient covariance factorization and reuse of intermediate values method.

Recent work such as [9, 13] show that exact NGD converges to the global optimum with a linear convergence rate. Work such as [15] analyze convergence for the Levenberg-Marquardt variant of NGD without specifying the convergence rate. The work in [9] provides the convergence analysis of KFAC for a shallow two-layer fully connected network where the convergence rate depends on the condition number of input data. Goldfarb *et al.* [12] follow the framework for stochastic quasi-Newton methods and prove that KBFGS converges with a sublinear rate for a network with bounded activation functions. TENGrAD improves the convergence properties of approximate NGD methods and has a linear convergence rate for DNNs with non-smooth activation functions.

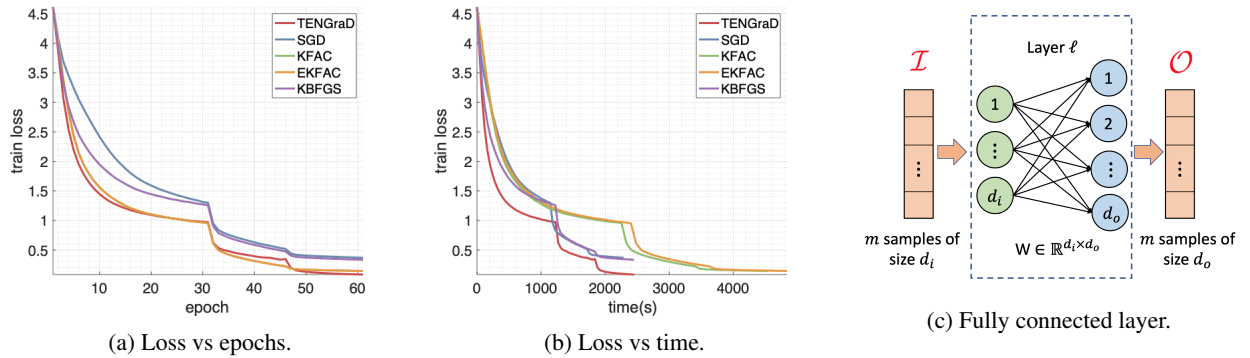


Figure 1: Training loss vs epoch and time for CIFAR-100 on DenseNet, and a fully connected layer.

Motivation and contributions: Figure 1a and Figure 1b show the performance of approximate NGD methods (including TENGrAD) and SGD for an image classification benchmark on a DNN. As shown in Figure 1a, the NGD methods provide more accurate updates resulting in a better loss reduction compared to SGD. However, as shown in Figure 1b, despite efforts made by approximate NGD methods to improve the overall time, none are competitive with tuned SGD with momentum. TENGrAD is the first NGD based implementation, which we call a time-efficient implementation, that outperforms other approximate NGD methods as well as SGD (under certain conditions) in overall time while benefiting from the convergence properties of second-order methods.

In the following, we demonstrate for a fully connected layer shown in Figure 1c, why TENGrAD is more time-efficient compared to state-of-the-art approximate NGD methods. Figure 2 shows KFAC, EKfAC, KBFGS, and TENGrAD. All methods first use a block-approximate approach to create the blocked matrix F_ℓ . KFAC, EKfAC, and KBFGS approximate F_ℓ with a Kronecker product of two Kronecker factors A and B . Because the size of factors is proportional to the input and output dimension of a layer, i.e. d_i and d_o , their inversion is costly to compute for wide layers and is cubic in input and output dimensions, i.e. $\mathcal{O}(d_i^3 + d_o^3)$. EKfAC creates factors U_A and U_B with a complexity that is also cubic in input and output dimensions of a layer. It also computes the scaling factor S by performing m number of matrix multiplications with the SVD factors. The rank-2 BFGS updates in KBFGS lead to a computation complexity that is quadratic in the input and output size of a layer.

TENGrAD computes the exact inverse of Fisher-blocks using the Woodbury matrix identity so the inverse is factorized into matrices C_1 and C_2 using a novel method called *covariance factorization*. The size of C_1 and C_2 is equal to a

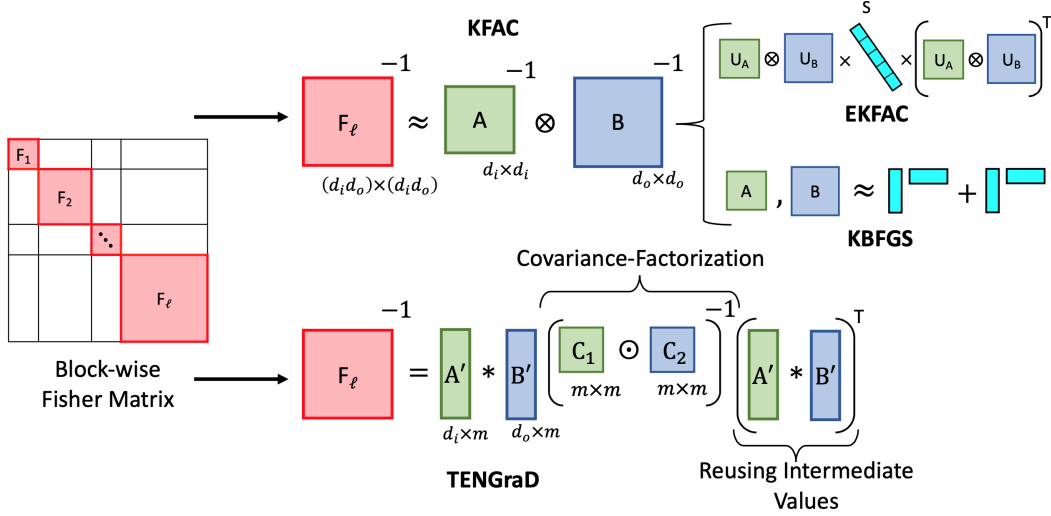


Figure 2: The TENGraD method vs Kronecker-factored approaches for a fully connected layer.

mini-batch size, i.e. $m \times m$, which is typically in the order of hundreds hence considerably smaller and easier to invert compared to Kronecker factors in other NGD methods. Other matrices, i.e. A' and B' , involved in the Fisher-block inverse in TENGraD, are *reused*. This accelerates the inverse computation as it removes extra passes on the network via storing intermediate values computed during the forward-backward passes. As a result, TENGraD becomes an actual time-efficient approximate NGD method and improves the overall time. Also, to the best of our knowledge, we are the first to prove the linear rate convergence of approximate NGD methods for deep neural networks with ReLU activation functions. Our contributions are:

- A time-efficient NGD method called TENGraD that computes the exact inverse of Fisher blocks efficiently by using a *covariance factorization* and *reuse* technique. Extension of TENGraD to convolutional layers using tensor algebra.
- Empirical demonstration that TENGraD outperforms overall time of state-of-the-art NGD methods and SGD on well-known deep learning benchmarks.
- TENGraD converges to the global optimum with a linear rate if exact gradients are used with an iteration complexity of $\mathcal{O}(\log(1/\epsilon))$ which is comparable to exact NGD methods.

2 Background and Definitions

A deep neural network transforms its input x to an output $f(\mathbf{W}; x)$ through a series of L layers where \mathbf{W} is the vector of network parameters. During the forward pass, layer l performs a linear transformation on its input of m samples, i.e. $\mathcal{I}_l \in \mathbb{R}^{d_i \times m}$, parameterized with $\mathbf{W}_l \in \mathbb{R}^{d_i \times d_o}$, and computes its outputs or *pre-activations*, $\mathcal{O}_l = \mathbf{W}_l^\top \mathcal{I}_l$, followed by a nonlinear activation function such as ReLU. The optimal parameters are obtained by minimizing the average loss \mathcal{L} over the training set during the backward pass:

$$\mathcal{L}(\mathbf{W}) = \frac{1}{n} \sum_{i=1}^n \ell(f(\mathbf{W}; \mathbf{x}_i), \mathbf{y}_i) \quad (1)$$

where $\mathbf{W} \in \mathbb{R}^p$ is the vector containing all of the network's parameters concatenated together, i.e. $[\text{vec}(\mathbf{W}_1)^\top \text{vec}(\mathbf{W}_2)^\top \dots \text{vec}(\mathbf{W}_L)^\top]^\top$, $\text{vec}(M)$ is the operator which vectorizes matrix M by stacking columns together, and ℓ measures the accuracy of the prediction (e.g. cross entropy loss).

Gradient and Jacobian in DNN. Optimization methods that aim to minimize the average loss in Equation 1 work with gradient computations. The average gradient over mini-batch m is defined as $\mathbf{g} = \frac{1}{m} \sum_{i=1}^m \nabla_{\mathbf{W}} \ell(f(\mathbf{W}; \mathbf{x}_i), \mathbf{y}_i)$ which is obtained using standard backpropagation. In the backpropagation, each layer l receives the gradient w.r.t its output, i.e. the *pre-activation derivatives* $\mathcal{G}_l \in \mathbb{R}^{d_o \times m}$, and computes the gradient w.r.t its parameters, i.e. $\mathbf{g}_l = \frac{1}{m} \mathcal{I}_l \mathcal{G}_l^\top$. The Jacobian of loss w.r.t the parameters for a single output network is defined as $\mathbf{J} = [\mathbf{J}_1^\top, \dots, \mathbf{J}_n^\top]^\top \in \mathbb{R}^{n \times p}$ where \mathbf{J}_i is the gradient of loss w.r.t the parameters. In the stochastic setting, for a layer l the Jacobian of loss w.r.t the layer parameters is approximated via $\mathbf{J}_l = (\mathcal{I}_l * \mathcal{G}_l)^\top \in \mathbb{R}^{m \times d_i d_o}$.

NGD update rule. Natural gradient descent scales the gradient with the inverse of FIM as follows:

$$\mathbf{W}(k+1) = \mathbf{W}(k) - \eta (\mathbf{F}(\mathbf{W}(k)) + \alpha \mathbf{I})^{-1} \mathbf{g}(k) \quad (2)$$

where η is the learning rate, α is the damping parameter, \mathbf{F} is the FIM of the model’s conditional distribution $P_{\mathbf{y}|\mathbf{x}}$ and is defined as $\mathbf{F} = \mathbb{E}_{P(\mathbf{x},\mathbf{y})} [\nabla_{\mathbf{W}} \log p_{\mathbf{W}}(\mathbf{y}|\mathbf{x}) \nabla_{\mathbf{W}} \log p_{\mathbf{W}}(\mathbf{y}|\mathbf{x})^\top]$ where $p_{\mathbf{W}}$ is the model’s density function. Since \mathbf{F} is singular for over-parameterized models, a non-negative damping term α is added to make it invertible. As shown in [5], the FIM coincides with Gauss-Newton matrix if the conditional distribution is in the exponential family which implies:

$$\mathbf{F}(\mathbf{W}(k)) = \frac{1}{m} \sum_{i=1}^n \nabla_{\mathbf{W}} \ell_i \nabla_{\mathbf{W}} \ell_i^\top \Big|_{\mathbf{W}=\mathbf{W}(k)} = \frac{1}{n} \mathbf{J}(k)^\top \mathbf{J}(k) \quad (3)$$

where $\ell_i = \ell(f(\mathbf{W}; \mathbf{x}_i), \mathbf{y}_i)$, $\mathbf{J}(k) = [\mathbf{J}_1(k)^\top, \dots, \mathbf{J}_n(k)^\top]^\top$ and $\mathbf{J}_i(k) = \nabla_{\mathbf{W}} \ell_i \Big|_{\mathbf{W}=\mathbf{W}(k)}$. Hereafter, we use $\mathbf{F}(k) = \mathbf{F}(\mathbf{W}(k))$ to simplify the notations.

Notations. Following notations are used in the paper: $[L] := \{1, \dots, L\}$, $\text{Diag}_{i=[L]}(A_i)$ is the block diagonal matrix with matrices $\{A_1, \dots, A_L\}$ on its diagonal; $\mathbf{X} \in \mathbb{R}^{n \times d}$ is the input data, i.e. $\mathbf{X} = [x_1, \dots, x_n]^\top$. $\lambda_{\min}(M)$ is the smallest eigenvalue of matrix M ; Hadamard product between two matrices is \odot ; the Kronecker product is \otimes ; $\|\cdot\|_2$ for the Euclidean norm of vectors/matrices; and $*$ is for the column-wise Khatri-Rao product; $A_{\cdot i}$ is used to denote the i -th columns of matrix A .

3 Time-Efficient NGD with Exact Fisher-block Inversion

The computation bottleneck in NGD is $(\mathbf{F}(k) + \alpha \mathbf{I})^{-1}$ and its gradient product. Naively computing the Fisher inverse is impractical due to its large size, i.e. p^2 where p is the number of parameters and can be millions. Therefore, the Fisher matrix is typically approximated with a block-diagonal matrix $\hat{\mathbf{F}} = \text{Diag}(\mathbf{F}_1, \dots, \mathbf{F}_L)$ where block \mathbf{F}_l corresponds to layer l [8]. As a result, $(\hat{\mathbf{F}} + \alpha \mathbf{I})^{-1}$ becomes a block diagonal matrix. TENGraD computes the exact inverse of each block, i.e. $(\mathbf{F}_l + \alpha \mathbf{I})^{-1}$ (hereafter, all computations are performed on one block, thus, l is removed from notations). TENGraD uses the Woodbury identity for each Fisher-block:

$$\mathbf{W}(k+1) = \mathbf{W}(k) - \frac{\eta}{\alpha} \left(\mathbf{g}(k) - \underbrace{\frac{\mathbf{J}(k)^\top}{m}}_C \underbrace{\left(\frac{\mathbf{J}(k)\mathbf{J}(k)^\top}{m} + \alpha \mathbf{I} \right)^{-1}}_A \underbrace{\mathbf{J}(k)\mathbf{g}(k)}_B \right) \quad (4)$$

where \mathbf{W} , \mathbf{g} , and \mathbf{J} are the parameters, gradient, and Jacobian associated with the Fisher-block (we drop the index k to simplify the notations). Main steps of the new update rule are: (A) computing and inverting the *Gram Jacobian* $\mathbf{J}\mathbf{J}^\top$, which is costly because the Jacobian \mathbf{J} and a matrix-matrix multiplication have to be computed, (B) scaling of the gradient $\mathbf{g}(k)$ using the Jacobian to transform the gradient into input space, and (C) rescaling with \mathbf{J}^\top to transform back to the parameter space. The Gram matrix $\mathbf{J}\mathbf{J}^\top$ computation in (A) has high complexity and is proportional to both input and output dimensions of a layer, i.e. $\mathcal{O}(md_i d_o)$. TENGraD mitigates this cost with *covariance factorization* that factors the Gram Jacobian into a low-cost operation between two small matrices. Steps (B) and (C) also involve Jacobian vector products that are orders of magnitude more computationally expensive than a gradient computation [14]. TENGraD mitigates this cost by *reusing* the input and activations computed during the forward-backward pass.

3.1 Covariance Factorization and Reusing of Intermediate Values in TENGraD

TENGraD factors the Gram matrix $\mathbf{J}\mathbf{J}^\top$ into two smaller $m \times m$ matrices C_1 and C_2 called covariance factors such that $\mathbf{J}\mathbf{J}^\top = C_1 \odot C_2$, m is the batch size. These factors can be obtained with low overhead as batch size is typically small. The basic method for computing the factors was first introduced in [15] for fully connected networks which we also add here for the sake of completeness. For only one sample and for the fully connected layer in Figure 1c, with the input \mathcal{I} and the pre-activations $\mathcal{O} = \mathbf{W}^\top \mathcal{I}$, we show the low-rank property of the gradient and how it is leveraged to reduce the computation complexity of the Gram Jacobian. The gradient of the loss w.r.t parameter θ_l for input sample i is computed using the input and pre-activation derivatives by $\mathbf{g}_i = \mathcal{I}_{\cdot i} \mathcal{G}_{\cdot i}^\top$. The gradient \mathbf{g}_i is the outer product of two vectors and therefore a rank-one matrix. The (i, j) element of Gram Jacobian is the inner product of vectorized gradients of two samples i and j , i.e. $[\mathbf{J}\mathbf{J}^\top]_{(i,j)} = \langle \text{vec}(\mathbf{g}_i), \text{vec}(\mathbf{g}_j) \rangle$. With $\text{vec}(uv^\top) = v \otimes u$, the Gram Jacobian becomes $[\mathbf{J}\mathbf{J}^\top]_{i,j} = \langle \mathcal{I}_{\cdot i} \otimes \mathcal{G}_{\cdot i}, \mathcal{I}_{\cdot j} \otimes \mathcal{G}_{\cdot j} \rangle$ and with $\langle u_1 \otimes v_1, u_2 \otimes v_2 \rangle = u_1^\top u_2 \cdot v_1^\top v_2$, it is rewritten as $[\mathbf{J}\mathbf{J}^\top]_{i,j} = \mathcal{I}_{\cdot i}^\top \mathcal{I}_{\cdot j} \cdot \mathcal{G}_{\cdot i}^\top \mathcal{G}_{\cdot j}$. As a result, the (i, j) -th element of the Gram Jacobian is efficiently computed without forming the gradients. Extended to a mini-batch of m samples, the per-sample gradients are written as the column-wise

Khatri-Rao product of input and pre-activation derivatives, i.e. $\mathbf{J} = (\mathcal{I} * \mathcal{G})^\top$. Therefore the compact form of the Gram Jacobian is:

$$\mathbf{J} = (\mathcal{I} * \mathcal{G})^\top \Rightarrow \mathbf{J}\mathbf{J}^\top = (\mathcal{I} * \mathcal{G})^\top (\mathcal{I} * \mathcal{G}) = \underbrace{\mathcal{I}^\top \mathcal{I}}_{C_1} \odot \underbrace{\mathcal{G}^\top \mathcal{G}}_{C_2} \quad (5)$$

From Equation 5, the Gram Jacobian is written as the Hadamard product of two smaller $m \times m$ matrices, i.e. covariance factors. The input covariance C_1 and the pre-activation covariance C_2 are efficiently computed during the forward and backward pass of the neural network using a matrix-matrix multiplication. The Jacobian does not need to be explicitly formed to compute these factors, reducing the overall computation complexity. Also, these factors are smaller and have low storage costs compared to Kronecker-factors, which have a size of $d_i \times d_i$ and $d_o \times d_o$.

The cost of storing the Jacobian for the NGD update in steps (B) and (C) of Equation 4 is considerable because its storage cost is m times the number of parameters. With a reuse method, TENGraD instead recomputes the Jacobian when needed, with a negligible computation cost and by storing small data structures. TENGraD breaks down the computation of Jacobian vector products in steps (B) and (C) into two operations involving input and pre-activation derivative matrices \mathcal{I} and \mathcal{G} . In step (B) in Equation 4 the vectorized form of the gradient for the layer parameters, i.e. $v = \text{vec}(\mathbf{g}(k))$, is propagated. The objective is to compute $\mathbf{J}\text{vec}(\mathbf{g}(k))$ without explicitly forming the Jacobian. With $\mathbf{J} = (\mathcal{I} * \mathcal{G})^\top$ and using the properties of column-wise Khatri-Rao product:

$$\mathbf{J}\text{vec}(\mathbf{g}(k)) = (\mathcal{I} * \mathcal{G})^\top \text{vec}(\mathbf{g}(k)) = ((\mathbf{g}(k)^\top \mathcal{I}) \odot \mathcal{G}) \mathbf{1}, \quad (6)$$

where $\mathbf{1}$ is a vector of all ones with appropriate dimension. The Jacobian vector product can be computed with two efficient matrix operations without forming the Jacobian. First, v_1 is computed with $v_1 = \mathbf{g}(k)^\top \mathcal{I}$, followed by a Hadamard product with the pre-activation derivative matrix, i.e. $v_2 = v_1 \odot \mathcal{G}$, and a column-wise summation on v_2 . In (C) in (4), the objective is to compute $\mathbf{J}^\top v$ with $v \in \mathbb{R}^m$ obtained from step (A). Using the column-wise Khatri-Rao structure of \mathbf{J} :

$$\mathbf{J}^\top v = (\mathcal{I} * \mathcal{G}) v = \mathcal{I} (v \mathbf{1}^\top \odot \mathcal{G}^\top). \quad (7)$$

Similarly, $\mathbf{J}^\top v$ is computed using the two step process in Equation 7. By storing I and G , TENGraD can efficiently compute the required operations in the NGD update.

Storage and Computation Complexity. Table 1 shows the computation and storage complexity of TENGraD vs other NGD methods. *Curvature* shows the cost of computing and inverting Kronecker-factors for KFAC, EKfAC, and KBFGS, and Gram Jacobian for TENGraD. The computation complexity of covariance factors is $\mathcal{O}(m^2(d_i + d_o))$, while Kronecker factors in KFAC have a complexity of $\mathcal{O}(md_i^2 + md_o^2)$. Inverting the factors in TENGraD is $\mathcal{O}(m^3)$ while that of KFAC is $\mathcal{O}(d_i^3 + d_o^3)$. Thus, when the batch size is smaller than layer dimensions TENGraD’s computation complexity is better than others. TENGraD reduces storage complexity with reuse from $\mathcal{O}(md_i d_o)$ to $\mathcal{O}(m(d_i + d_o))$, see the *Extra Storage* column. *Extra Pass* refers to the cost of a second backpropagation and *Step* is the computation cost of parameter updates after computing the curvature.

Table 1: Computation and storage complexity of NGD methods.

Algorithm	Curvature	Extra Pass	Step	Extra Storage
TENGraD	$\mathcal{O}(m^2 d_i + m^2 d_o + m^3)$	$\mathcal{O}(m d_i d_o)$	$\mathcal{O}(m d_i d_o + m d_o + m^2)$	$\mathcal{O}(m d_i + m d_o + m^2)$
KFAC	$\mathcal{O}(m d_i^2 + m d_o^2 + d_i^3 + d_o^3)$	$\mathcal{O}(m d_i d_o)$	$\mathcal{O}(d_i^2 d_o + d_o^2 d_i)$	$\mathcal{O}(d_i^2 + d_o^2)$
EKfAC	$\mathcal{O}(m d_i^2 + m d_o^2 + d_i^3 + d_o^3)$	$\mathcal{O}(m d_i d_o)$	$\mathcal{O}(m d_o d_i^2 + m d_o^2 d_i)$	$\mathcal{O}(m d_i d_o + d_i^2 + d_o^2)$
KBFGS	$\mathcal{O}(m d_i^2 + m d_o^2 + d_i^2)$	$\mathcal{O}(m d_i d_o)$	$\mathcal{O}(d_i^2 d_o + d_o^2 d_i)$	$\mathcal{O}(d_i^2 + d_o^2)$

3.2 Extension to Convolution Layers

We extend TENGraD to support convolutional layers, general form provided in the Appendix. Convolutional layers operate on high-dimension tensors. For a general tensor $\mathcal{A} \in \mathbb{R}^{N_1 \times \dots \times N_p}$ with dimension p , the components of a tensor can be represented with $\mathcal{A}_{i_1, \dots, i_p}$ where index i_α is associated with dimension α . We consider a convolutional layer with the input tensor $\mathcal{I} \in \mathbb{R}^{c_{in} \times w_{in} \times h_{in}}$ and convolutional filters $\mathcal{W} \in \mathbb{R}^{c_{in} \times d \times d \times c_{out}}$. For the weight tensor \mathcal{W} the spatial support of each kernel filter is $d \times d$. There are c_{in} input channels and c_{out} feature maps. Let $\mathcal{O} \in \mathbb{R}^{c_{out} \times w_{out} \times h_{out}}$ be the output of the convolutional layer, where $w_{out} = \lfloor w_{in} + 2p_d - d \rfloor / s + 1$ and $h_{out} = \lfloor h_{in} + 2p_d - d \rfloor / s + 1$. Also, p_d and s are the padding and stride parameters, respectively.

To extend covariance factorization for $\mathbf{J}\mathbf{J}^\top$ in a convolutional layer, we first derive a closed form equation for the Jacobian and show that the convolution operation can be written as a matrix multiplication for a single sample. From Figure 3, \mathcal{I} can be reshaped to a matrix I with dimensions $(w_{out} \times h_{out}) \times (c_{in} \times d \times d)$, each row is an unfolded sub-tensor in I that has the same size of a group of c_{in} filters. Each c_{in} filter is also unfolded into a 1-D vector with

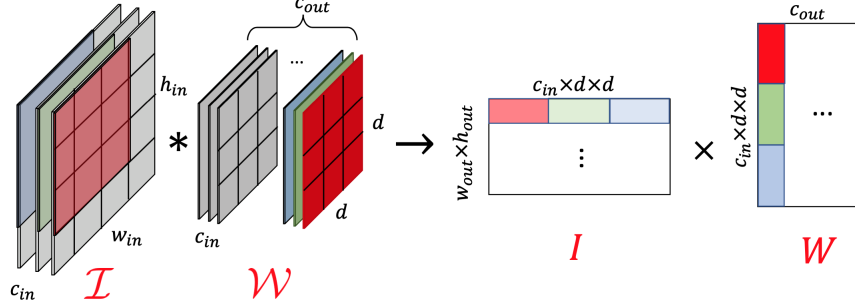


Figure 3: Convolution shown as matrix-matrix product of unfolded input and weights.

size $(c_{in} \times d \times d) \times 1$. The weight tensor \mathcal{W} is reshaped to a matrix W with size $(c_{in} \times d \times d) \times c_{out}$ (see Figure 3). Hence, convolution can be written as $O = I \cdot W$, where the shape of O is $(w_{out} \times h_{out}) \times (c_{out})$. Matrix O is reshaped to the output tensor $\mathcal{O} \in \mathbb{R}^{c_{out} \times w_{out} \times h_{out}}$ by folding each column into a $w_{out} \times h_{out}$ feature map. Applying a similar unfolding to the pre-activation derivatives tensor $\mathcal{G} \in \mathbb{R}^{c_{out} \times w_{out} \times h_{out}}$ results in the matrix G with a shape of $(w_{out} \times h_{out}) \times (c_{out})$.

The compact form of the Jacobian for a batch of m samples, with $O = I \cdot W$, is:

$$\mathbf{J} = [\text{vec}(\mathbf{g}_1), \dots, \text{vec}(\mathbf{g}_m),] = [\text{vec}(I_1^\top \cdot G_1), \dots, \text{vec}(I_m^\top \cdot G_m)]^\top \quad (8)$$

where I_i and G_i are the unfolded input and output for sample i . We derive a closed form for an arbitrary element (i, j) in the Gram Jacobian matrix and then extend to the whole batch size. Using Equation 8 each element in the Gram Jacobian is written as:

$$[\mathbf{J}\mathbf{J}^\top]_{i,j} = \langle \text{vec}(I_i^\top \cdot G_i), \text{vec}(I_j^\top \cdot G_j) \rangle = \mathbf{1}^\top I_i I_j^\top \cdot G_i G_j^\top \mathbf{1} \quad (9)$$

Hence, each element (i, j) in Gram Jacobian is obtained via a reduction on covariance matrices $I_i I_j^\top \in \mathbb{R}^{(w_{out} \times h_{out}) \times (w_{out} \times h_{out})}$ and $G_i G_j^\top \in \mathbb{R}^{(w_{out} \times h_{out}) \times (w_{out} \times h_{out})}$. The covariance matrices are defined over the spatial support $S = w_{out} \times h_{out}$.

With tensor notations, we expand the dimensions of covariance factors. Since element (i, j) in Gram Jacobian is represented with two covariance matrices, the $m \times m$ Gram Jacobian is m^2 covariance matrices. The covariance tensors $C_1 \in \mathbb{R}^{m \times m \times S \times S}$ and $C_2 \in \mathbb{R}^{m \times m \times S \times S}$ are defined as:

$$[C_1]_{i,j,*,*} = I_i I_j^\top, \quad [C_2]_{i,j,*,*} = G_i G_j^\top \quad (10)$$

Where $[C_1]_{i,j,*,*}$ denotes the sub-tensor at (i, j) . As a result the Gram Jacobian is written as:

$$\mathbf{J}\mathbf{J}^\top = \sum_{s \in S} \sum_{s' \in S} [C_1 \odot C_2]_{*,*,s,s'} \quad (11)$$

Corollary 1 For a standard convolutional layer with spatial support $S = w_{out} \times h_{out}$, overall filter support $F = c_{in} \times d \times d$ and batch size m , TENGraD reduces the computational complexity of the Gram Jacobian computation from $\mathcal{O}(m^2 F c_{out} + m F S c_{out})$ to $\mathcal{O}(m^2 S^2 (F + c_{out}))$.

For TENGraD's reuse for step (B), the gradient tensor of the convolution layer, i.e. $\mathbf{g}(k) \in \mathbb{R}^{c_{in} \times d \times d \times c_{out}}$ is reshaped to $\hat{\mathbf{g}}(k) \in \mathbb{R}^{(c_{in} \times d \times d) \times c_{out}}$ to compute $\mathbf{J}\mathbf{v} = \mathbf{J}\text{vec}(\hat{\mathbf{g}}(k))$. Using Equation 9, this can be written as a two step process without explicitly forming the Jacobian matrix: $[\mathbf{J}\mathbf{v}]_i = \mathbf{1}^\top (G_i \cdot \hat{\mathbf{g}}(k)^\top \odot I_i) \mathbf{1}$. Similarly, for step (C), $\mathbf{J}^\top \mathbf{v}$ for $\mathbf{v} \in \mathbb{R}^m$ is computed with $\mathbf{J}^\top \mathbf{v} = \sum_{i=1}^m I_i^\top (G_i \cdot \mathbf{v}_i)$. For better storage, instead of I we store the input tensor \mathcal{I} .

4 Linear Convergence in TENGraD

We provide convergence guarantees for TENGraD with exact gradients (i.e. full batch case with $m = n$). We focus on the single output but a general case with multiple outputs will be similar. As shown TENGraD, converges linearly at a rate independent from the condition number of the input data matrix $\mathbf{X}^\top \mathbf{X}$, unlike the convergence rate provided for KFAC at [9]. Consequently, for sufficiently ill-conditioned data, our convergence guarantees will improve upon those currently available for KFAC.

Lets us introduce the output vector $\mathbf{u}(\mathbf{W}) = [u_1(\mathbf{W}), \dots, u_n(\mathbf{W})]^\top$ where $u_i(\mathbf{W}) = f_L(\mathbf{W}; x_i)$ and $y = [y_1, \dots, y_n]^\top$. We consider the squared error loss \mathcal{L} on a given dataset $\{x_i, y_i\}_{i=1}^n$ with $x_i \in \mathbb{R}^d$ and $y_i \in \mathbb{R}$, i.e. the objective is to minimize $\min_{\mathbf{W} \in \mathbb{R}^p} \mathcal{L}(\mathbf{W}) = \frac{1}{2} \|\mathbf{u}(\mathbf{W}) - y\|^2$. The update rule (4) of TENGraD with exact gradient becomes

$$\mathbf{W}(k+1) = \mathbf{W}(k) - \eta \left(\hat{\mathbf{F}}(\mathbf{W}(k)) + \alpha \mathbf{I} \right)^{-1} \mathbf{J}(k)^\top (\mathbf{u}(\mathbf{W}(k)) - y), \quad (12)$$

where $\hat{\mathbf{F}}(\mathbf{W}(k)) := \hat{\mathbf{J}}(k)^\top \hat{\mathbf{J}}(k)$ is the Fisher-block matrix and the block Jacobian is defined as $\hat{\mathbf{J}}(k) = \text{Diag}_{l \in [L]}(J_l(k))$ for $J_l(k) := \left(\frac{\partial \mathbf{f}(\mathbf{W}(k))}{\partial \text{vec}(\mathbf{W}_l)} \right)$ and $\mathbf{f}(\mathbf{W}) = [f_L(\mathbf{W}; x_1), \dots, f_L(\mathbf{W}; x_n)]^\top$. It can be seen directly from the TENGraD update rule (4) that if the Gram matrix $G_l(k) := J_l(k)J_l(k)^\top$ stays positive definite and bounded for each layer l and iteration k , then by the standard theory of preconditioned gradient descent methods [22], it will converge globally for sufficiently small stepsizes. In the following, we introduce two assumptions; the first one ensures that at the initialization Gram matrix is positive-definite and the second assumption is a stability condition on the Jacobian requiring that it does not vary too rapidly. These assumptions will allow us to control the convergence rate.

Assumption 1 *The data X is normalized, $|y_i| = \mathcal{O}(1)$, and for any $i \neq j$, x_i and x_j are independent. Lastly, the Gram matrix for individual layers are positive definite at initialization, i.e. $\min_{l \in [L]} \lambda_{\min}(G_l(0)) = \lambda_0 > 0$.*

Lee et al. [23] shows that if the input data are i.i.d. samples, then Assumption 1 can often be satisfied.

Assumption 2 *There exists $0 < C \leq \frac{1}{2}$ that satisfies $\|\mathbf{J}(\mathbf{W}(k)) - \mathbf{J}(\mathbf{W}(0))\|_2 \leq \frac{C}{3} \lambda_0^{\frac{1}{2}}$ if $\|\mathbf{W}(k) - \mathbf{W}(0)\|_2 \leq 3\lambda_0^{-\frac{1}{2}} \|\mathbf{y} - \mathbf{u}(0)\|_2$.*

Notice that Assumption 2 requires that the network behaves like a linearized network for small values of constant C [23]. As a result of Assumptions 1-2, the Fisher block matrix remains close to the initialization over iterations and therefore the Gram matrices of layers stay positive-definite during training which is parallel to the setting of [9, 24, 25]. In practice, we could also keep Gram matrices well-conditioned during training by tuning the damping parameter.

Next, we present our convergence result in Theorem 1. Our analysis follows the techniques of [9] and adapts them for TENGraD. Notice that TENGraD differs from NGD and KFAC in terms of the matrix it uses to approximate FIM; therefore results of [9] do not directly apply to our setting. As a proof technique, we first utilize the Assumptions 1 and 2 to derive a lower bound on the smallest eigenvalue λ_0 of the Fisher-block matrix $\hat{\mathbf{F}}$ showing that it is positive, and building on this result we derive the rate in the following result. The proof can be found in the Appendix.

Theorem 1 *Suppose Assumptions 1, 2 hold. Consider the update rule (12) for a network with L layers, damping parameter $0 < \alpha \leq \frac{4\lambda_0}{9n}$, and learning rate $\eta \in (0, \frac{2L\gamma-1-2C\sqrt{L}\gamma}{(L+C\sqrt{L}\gamma)^2})$ where $\gamma = \frac{\lambda_0}{\lambda_0 + \frac{9}{4}n\alpha}$. Then, we have $\|\mathbf{u}(k) - y\|_2^2 \leq (1 - \eta)^k \|\mathbf{u}(0) - y\|_2^2$.*

Theorem 1 states that TENGraD converges to the global optimum with a linear rate under Assumptions 1 and 2. Therefore, TENGraD requires only $\mathcal{O}(\log(1/\epsilon))$ iterations to achieve ϵ accuracy. Moreover, our result shows that a smaller learning rate is needed for a deeper network to guarantee linear convergence. This behavior is different than that of exact NGD because the rate of exact NGD provided in [9] does not depend on the network size but rather on the parameter C . We also observe from Theorem 1 that smaller damping parameter improves the upper bound on the learning rate which suggests faster convergence for TENGraD. This makes the analysis of λ_0 important for the performance of TENGraD since Gram matrix can potentially be ill-conditioned. The work [9] uses matrix concentration inequalities and harmonic analysis techniques to bound the minimum eigenvalue of the Gram matrix of the L -layer ReLU network which does not provide a tight bound for the Gram matrix of each layer. The authors of [25] have obtained tighter bounds in the NTK setting, and their result can be used to derive lower bound on λ_0 of $\hat{\mathbf{J}}_l \hat{\mathbf{J}}_l(k)^\top$. Due to limited space, we present the details on the explicit bound on λ_0 at Appendix.

We can show that under some mild conditions on the distribution of input data X , if the weights of layer l are drawn from $\mathcal{N}(0, \beta_l^2)$, and the conditions $d_l = \tilde{\Omega}(N)$ and $\prod_{j=1}^{l-2} \log(d_j) = o(\min_{j \in [0, l-1]} d_j)$ are satisfied, then the smallest eigenvalue of Gram matrix $\hat{\mathbf{J}}_l(k) \hat{\mathbf{J}}_l(k)^\top$ satisfies $\lambda_{\min}(\hat{\mathbf{J}}_l(k) \hat{\mathbf{J}}_l(k)^\top) \geq C_\beta \Omega(\prod_{l=1}^L d_l)$ for all $k > 0$ with some probability where the coefficient C_β depends on the variances β_l^2 (see Appendix). This implies that we can choose a smaller damping parameter α to get a faster rate according to Theorem 1 which, in turn, improves the performance of TENGraD. Otherwise, α needs to be larger to guarantee the inversion at (12).

5 Experimental Results

We test TENGraD, KFAC, EKfAC, KBFgs, and SGD with momentum on three image classification benchmarks namely Fashion-MNIST [26], CIFAR-10[27] and CIFAR-100 [27]. For Fashion-MNIST a network with its

convolution layers and one fully connected layer is used, hence called 3C1F. For other benchmarks, the following DNN architectures are used DenseNet [28], WideResNet [29] and MobileNetV2 [30]. In all experiments, 50K samples are chosen for training and 10K for test. Experiments are conducted on AWS P3.2xlarge machines with one Volta V100 GPU and 16GB RAM. Each experiment is repeated 5 times and the average is reported. In our theoretical analysis, we assumed deterministic gradients but in the experiments we use stochastic gradients estimated with mini-batch size $m = 128$. The Appendix provides additional setup information.

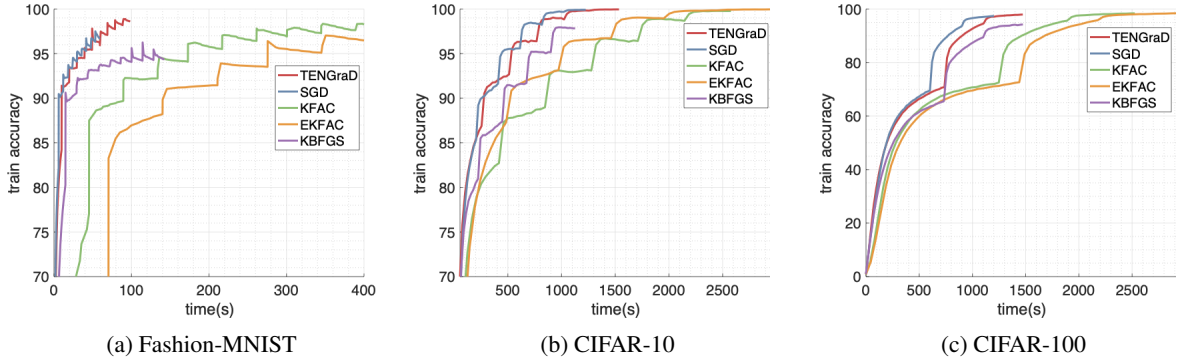


Figure 4: Comparing train accuracy between optimization methods for a) Fashion-MNIST on 3C1F network. b) CIFAR-10 on Wide-ResNet network c) CIFAR-100 on Wide-ResNet Network.

From the training loss plots in Figure 4, TENGraD clearly outperforms all other approximate NGD methods in timing and train accuracy. Moreover, TENGraD performs better than SGD in both time and accuracy on Fashion-MNIST dataset, as shown in Figure 4a, and it has a competitive timing compared to SGD on both CIFAR-10 and CIFAR-100 as shown in Figure 4b and Figure 4c. The test accuracy reported in Figure 5 shows that TENGraD also generalizes well and achieves state-of-the-art accuracy on all benchmarks, and especially outperforms KBFGS with a margin of 1.6%. Moreover, TENGraD clearly outperforms SGD in both time and test accuracy on Fashion-MNIST, as shown in Figure 5a, with competitive results on CIFAR-10 and CIFAR-100.

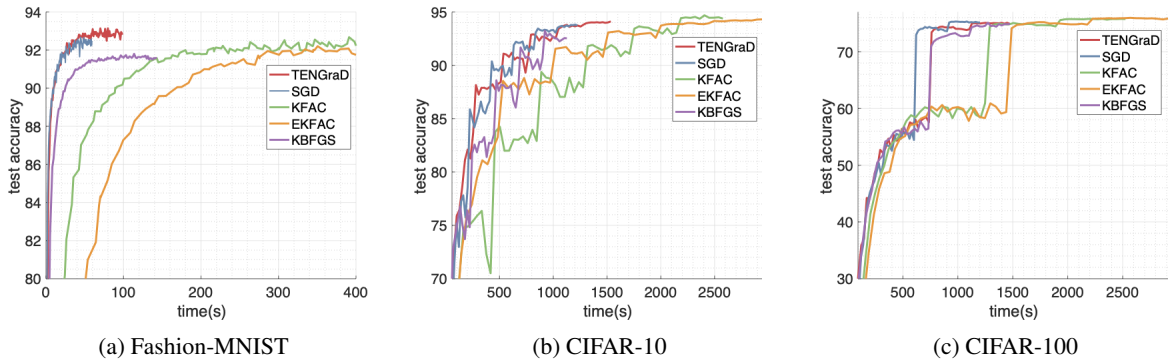


Figure 5: Comparing test accuracy between optimization methods for a) Fashion-MNIST on 3C1F network. b) CIFAR-10 on Wide-ResNet network c) CIFAR-100 on Wide-ResNet Network.

To further demonstrate the performance of TENGraD, we conduct extensive experiments on state-of-the-art DNNs and report the time and test accuracy for the 7 configurations in Table 2. Our results show that TENGraD outperforms KFAC, EKfAC, and KBFGS in overall time in 7 out of 7 (7/7) experiments. Moreover, TENGraD achieves a better accuracy, with a margin between 0.4%-1.41%, in 6/7 experiments compared to KBFGS which is the fastest method among approximate Kronecker-factored NGD methods. Also, compared to SGD, TENGraD achieves a better timing for 3/7 experiments and a better test accuracy in 5/7. In particular, TENGraD shows a 20% improvement over SGD in time for the Fashion-MNIST dataset and a better timing for CIFAR-10 on Wide-ResNet and DenseNet.

To compare the quality of Fisher matrix approximation, we compare the block-diagonal approximation in TENGraD and KFAC with exact NGD. From Figure 6, TENGraD provides a similar approximation to the exact NGD by preserving the structure of the Fisher matrix. However, KFAC’s approximation hardly captures the structure. Similar results for other layers are observed (see Appendix).

Table 2: Top test accuracy and time for state-of-the-art models and different natural gradient methods.

Models	Dataset	Time(s) [Accuracy%]				
		SGD	TENGrAD	KFAC	EKFAC	KBFGS
3CIF	F-MNIST	52 [92.60]	43 [93.15]	188 [92.2]	275 [92.01]	113 [92.12]
WideResNet	CIFAR-10	1128 [94.01]	1108 [94.10]	2454 [94.50]	2936 [94.10]	1132 [92.70]
	CIFAR-100	1004 [75.79]	1124 [75.20]	2419 [75.60]	2766 [76.07]	1151 [74.35]
DenseNet	CIFAR-10	2278 [93.52]	2077 [93.40]	4292 [93.31]	4820 [93.11]	2412 [93.41]
	CIFAR-100	1909 [72.10]	2002 [73.90]	3542 [74.50]	3788 [74.29]	2292 [73.50]
MobileNetV2	CIFAR-10	1350 [92.70]	1841 [92.71]	3221 [92.63]	4304 [92.83]	1728 [91.30]
	CIFAR-100	1370 [72.78]	1406 [72.81]	3152 [72.82]	4687 [72.97]	1695 [72.01]

To demonstrate the robustness, we examine the train accuracy under various hyperparameter (HP) settings and show TENGrAD is stable under a wide range for the HPs (see Appendix).

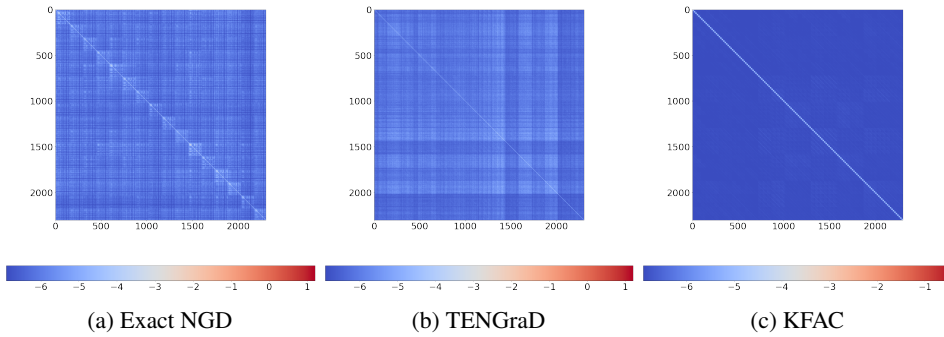


Figure 6: Structure of block inverses for the second convolution layer in 3CIF with Fashion-MNIST.

6 Conclusion

We propose a Time-Efficient NGD method, called TENGrAD, that improves the overall time of second order methods with computationally efficient factorization and reuse methods and prove linear convergence rates under certain assumptions. Extension to convolutional and general layers is provided. Results indicate that TENGrAD outperforms or perform comparably to the state-of-the-art NGD methods as well as SGD. Our work does not have a direct negative impact as it is mostly theoretical.

Acknowledgements

This work was supported in part by NSERC Discovery Grants (RGPIN-06516, DGEGR-00303), XSEDE, the Canada Research Chairs program, and NSF grants CCF-1814888, NSF DMS-2053485, NSF DMS-1723085 and Office of Naval Research Award Number N00014-21-1-2244.

References

- [1] Shun-Ichi Amari. Natural gradient works efficiently in learning. *Neural computation*, 10(2):251–276, 1998.
- [2] Shun-ichi Amari. Neural learning in structured parameter spaces - natural riemannian gradient. In M. C. Mozer, M. Jordan, and T. Petsche, editors, *Advances in Neural Information Processing Systems*, volume 9. MIT Press, 1997.
- [3] Tianle Cai. A gram-gauss-newton method learning overparameterized deep neural networks for regression problems. *Machine learning*, (1/28), 2019.
- [4] Ryo Karakida and Kazuki Osawa. Understanding approximate fisher information for fast convergence of natural gradient descent in wide neural networks. In H. Larochelle, M. Ranzato, R. Hadsell, M. F. Balcan, and H. Lin, editors, *Advances in Neural Information Processing Systems*, volume 33, pages 10891–10901. Curran Associates, Inc., 2020.

- [5] James Martens. New insights and perspectives on the natural gradient method. *Journal of Machine Learning Research*, 21(146):1–76, 2020.
- [6] Jeffrey Pennington and Pratik Worah. The spectrum of the fisher information matrix of a single-hidden-layer neural network. In S. Bengio, H. Wallach, H. Larochelle, K. Grauman, N. Cesa-Bianchi, and R. Garnett, editors, *Advances in Neural Information Processing Systems*, volume 31. Curran Associates, Inc., 2018.
- [7] Ryo Karakida, Shotaro Akaho, and Shun-ichi Amari. Universal statistics of fisher information in deep neural networks: Mean field approach. In *The 22nd International Conference on Artificial Intelligence and Statistics*, pages 1032–1041. PMLR, 2019.
- [8] Roger Grosse and James Martens. A kronecker-factored approximate fisher matrix for convolution layers. In *International Conference on Machine Learning*, pages 573–582. PMLR, 2016.
- [9] Guodong Zhang, James Martens, and Roger B Grosse. Fast convergence of natural gradient descent for over-parameterized neural networks. In H. Wallach, H. Larochelle, A. Beygelzimer, F. d'Alché-Buc, E. Fox, and R. Garnett, editors, *Advances in Neural Information Processing Systems*, volume 32. Curran Associates, Inc., 2019.
- [10] Herbert Robbins and Sutton Monro. A stochastic approximation method. *The annals of mathematical statistics*, pages 400–407, 1951.
- [11] Thomas George, César Laurent, Xavier Bouthillier, Nicolas Ballas, and Pascal Vincent. Fast approximate natural gradient descent in a kronecker factored eigenbasis. In S. Bengio, H. Wallach, H. Larochelle, K. Grauman, N. Cesa-Bianchi, and R. Garnett, editors, *Advances in Neural Information Processing Systems*, volume 31. Curran Associates, Inc., 2018.
- [12] Donald Goldfarb, Yi Ren, and Achraf Bahamou. Practical quasi-newton methods for training deep neural networks. In H. Larochelle, M. Ranzato, R. Hadsell, M. F. Balcan, and H. Lin, editors, *Advances in Neural Information Processing Systems*, volume 33, pages 2386–2396. Curran Associates, Inc., 2020.
- [13] Alberto Bernacchia, Mate Lengyel, and Guillaume Hennequin. Exact natural gradient in deep linear networks and application to the nonlinear case. NIPS, 2019.
- [14] Felix Dangel, Frederik Kunstner, and Philipp Hennig. Backpack: Packing more into backprop. In *International Conference on Learning Representations*, 2019.
- [15] Yi Ren and Donald Goldfarb. Efficient subsampled gauss-newton and natural gradient methods for training neural networks. *arXiv preprint arXiv:1906.02353*, 2019.
- [16] Frederik Kunstner, Philipp Hennig, and Lukas Balles. Limitations of the empirical fisher approximation for natural gradient descent. In H. Wallach, H. Larochelle, A. Beygelzimer, F. d'Alché-Buc, E. Fox, and R. Garnett, editors, *Advances in Neural Information Processing Systems*, volume 32. Curran Associates, Inc., 2019.
- [17] Aleksandar Botev, Hippolyt Ritter, and David Barber. Practical gauss-newton optimisation for deep learning. In *International Conference on Machine Learning*, pages 557–565. PMLR, 2017.
- [18] Tom Heskes. On “natural” learning and pruning in multilayered perceptrons. *Neural Computation*, 12(4):881–901, 2000.
- [19] Guillaume Desjardins, Karen Simonyan, Razvan Pascanu, and koray kavukcuoglu. Natural neural networks. In C. Cortes, N. Lawrence, D. Lee, M. Sugiyama, and R. Garnett, editors, *Advances in Neural Information Processing Systems*, volume 28. Curran Associates, Inc., 2015.
- [20] Sidak Pal Singh and Dan Alistarh. Woodfisher: Efficient second-order approximation for neural network compression. *Advances in Neural Information Processing Systems*, 33, 2020.
- [21] James Martens and Roger Grosse. Optimizing neural networks with kronecker-factored approximate curvature. In *International conference on machine learning*, pages 2408–2417. PMLR, 2015.
- [22] Dimitri P Bertsekas. Nonlinear programming. *Journal of the Operational Research Society*, 48(3):334–334, 1997.
- [23] Simon Du, Jason Lee, Haochuan Li, Liwei Wang, and Xiyu Zhai. Gradient descent finds global minima of deep neural networks. In Kamalika Chaudhuri and Ruslan Salakhutdinov, editors, *Proceedings of the 36th International Conference on Machine Learning*, volume 97 of *Proceedings of Machine Learning Research*, pages 1675–1685. PMLR, 09–15 Jun 2019.
- [24] Simon S Du, Xiyu Zhai, Barnabas Poczos, and Aarti Singh. Gradient descent provably optimizes over-parameterized neural networks. *arXiv preprint arXiv:1810.02054*, 2018.
- [25] Quynh Nguyen, Marco Mondelli, and Guido Montufar. Tight bounds on the smallest eigenvalue of the neural tangent kernel for deep relu networks. *arXiv preprint arXiv:2012.11654*, 2020.

- [26] Han Xiao, Kashif Rasul, and Roland Vollgraf. Fashion-mnist: a novel image dataset for benchmarking machine learning algorithms. *arXiv preprint arXiv:1708.07747*, 2017.
- [27] Alex Krizhevsky. Learning multiple layers of features from tiny images. Technical report, 2009.
- [28] Gao Huang, Zhuang Liu, Laurens Van Der Maaten, and Kilian Q Weinberger. Densely connected convolutional networks. In *Proceedings of the IEEE conference on computer vision and pattern recognition*, pages 4700–4708, 2017.
- [29] Sergey Zagoruyko and Nikos Komodakis. Wide residual networks. In *British Machine Vision Conference 2016*. British Machine Vision Association, 2016.
- [30] Mark Sandler, Andrew Howard, Menglong Zhu, Andrey Zhmoginov, and Liang-Chieh Chen. Mobilenetv2: Inverted residuals and linear bottlenecks. In *Proceedings of the IEEE conference on computer vision and pattern recognition*, pages 4510–4520, 2018.

A Appendix

A.1 Outline

The general form of the covariance factorization discussed in Section 3.2 is provided in Section A.2. The convergence proof of Theorem 1 discussed in Section 4 is provided in Section A.3.1. The bounds for minimum eigenvalue λ_0 discussed in Section 4 is provided in A.3.2. We provide the setup information in Section A.4.1. The plots that compare the quality of approximation of Fisher inverse blocks are provide in Section A.4.2. We provide the sensitivity to hyperparameters figures in Section A.4.3. For the error bars refer to Section A.5.

A.2 General From of Covariance Factorization

In this section, we extend the results obtained in Section 3 and show that the covariance factorization and reuse method can be applied to an arbitrary layer. An arbitrary layer can operate on its input tensor in many ways depending on its underlying linear transformations. Typically these transformations operate differently on each tensor dimension. For example, a transformation such as convolution applies a specific filtering on spatial dimensions. Therefore, we need to distinguish between these dimensions depending on the operations performed on them. In the following, we categorize these dimensions into free, independent, and common dimensions.

Tensor Dimensions. A *common dimension* is the dimension of the unfolded input that is shared amongst input and output tensors, i.e. spatial dimensions. An *independent dimension* is the dimension of the unfolded input that is shared amongst input and the parameters, i.e. input channel c_{in} and filter dimensions k . A *free dimension* is the dimension of the parameters that is shared amongst output and the parameters, i.e. output channel c_{out} .

Now, we show that the Jacobian matrix \mathbf{J} can be formed as a linear transformation amongst two tensors namely input and pre-activation derivatives which later is used to compute the Gram Jacobian $\mathbf{J}\mathbf{J}^\top$.

Lemma 1 Consider a layer with parameters θ_{v,i_1,\dots,i_k} that applies a linear transformation on input tensor $\mathcal{I}_{m,j_1,\dots,j_l}$ where v and m are the indices of free dimension and batch samples. Suppose that the output for a sample can be computed without requiring other samples, i.e. there is no dependency amongst samples in a batch. The pre-activation derivatives are given by tensor $\mathcal{G}_{m,v,t_1,\dots,t_p}$. We refer to set $\{t_1, \dots, t_p\}$ as common dimensions or M_C and $\{i_1, \dots, i_k\}$ as independent dimensions or M_I . Then the Jacobian tensor can be written as:

$$\mathcal{J}_{m,v,M_I} = \sum_{M_C} \mathcal{G}_{m,v,M_C} \hat{\mathcal{I}}_{m,M_C,M_I} \quad (13)$$

where tensor $\hat{\mathcal{I}}$ is obtained by unfolding the input tensor \mathcal{I} :

$$\hat{\mathcal{I}}_{m,M_C,M_I} = \sum_{j_\alpha \in \Omega} \mathcal{I}_{m,j_1,\dots,j_l} \quad (14)$$

where Ω depends on the underlying linear transformation.

Proof of Lemma 1. Assume the arbitrary linear transformation as follow:

$$\mathcal{O}_{m,v,t_1,\dots,t_p} = \sum_{j_\alpha \in \Omega, i_\beta \in \Gamma} \mathcal{I}_{m,j_1,\dots,j_p} \theta_{v,i_1,\dots,i_k} \quad (15)$$

Where Ω and Γ define the underlying linear transformation such as the input and filter spatial dimensions in the convolutional layer. Now, we can rewrite Equation 15 by unfolding the input tensor. To do so, for each index $i_\beta \in \Gamma$ we can unfold the input tensor using the following:

$$\hat{\mathcal{I}}_{m,t_1,\dots,t_p,i_1,\dots,i_k} = \sum_{j_\alpha \in \Omega} \mathcal{I}_{m,j_1,\dots,j_l} \quad (16)$$

The above equation unfolds the input along all the dimensions in the shared dimensions with the output tensor, i.e. M_C , and for all the dimensions in the parameter tensor. As a result, the output can be written as the following:

$$\mathcal{O}_{m,v,M_C} = \sum_{M_I} \hat{\mathcal{I}}_{m,M_C,M_I} \theta_{v,M_I} \quad (17)$$

Using this result and the fact that the pre-activation derivatives tensor \mathcal{G} has the same dimension as output tensor \mathcal{O} , we can obtain the Jacobian tensor \mathcal{J} as stated in the Equation 13.

Lemma 1 shows that the Jacobian tensor \mathcal{J} can be achieved with a linear transformation between the unfolded input tensor $\hat{\mathcal{I}}$ and the pre-activation derivative tensor \mathcal{G} . Now, using this result we can extend the covariance factorization in TENGraD to an arbitrary layer.

Theorem 2 For a linear layer with input tensor \mathcal{I} and pre-activation derivatives \mathcal{G} defined in Lemma 1, the Gram matrix $\mathbf{J}\mathbf{J}^\top$ is obtained by:

$$\mathbf{J}\mathbf{J}^\top = \sum_{M_C} \sum_{M'_C} C_1 \odot C_2$$

where C_1 and C_2 are the covariance tensors of unfolded input and pre-activation derivatives defined as:

$$\begin{aligned} [C_1]_{m,m',M_C,M'_C} &= \sum_{M_I} \hat{\mathcal{I}}_{m,M_C,M_I} \hat{\mathcal{I}}_{m',M'_C,M_I} \\ [C_2]_{m,m',M_C,M'_C} &= \sum_v \mathcal{G}_{m,v,M_C} \mathcal{G}_{m',v,M'_C} \end{aligned}$$

Proof of Theorem 2. Using Lemma 1 we can write the Gram Jacobian matrix by expanding the common dimensions as follows:

$$\begin{aligned} \mathbf{J}\mathbf{J}^\top &= \sum_v \sum_{M_I} \mathcal{J}_{m,v,M_I} \mathcal{J}_{m',v,M_I} \\ &= \sum_{M_C} \sum_{M'_C} \sum_v \sum_{M_I} \mathcal{G}_{m,v,M_C} \mathcal{G}_{m',v,M'_C} \hat{\mathcal{I}}_{m,M_C,M_I} \hat{\mathcal{I}}_{m',M'_C,M_I} \\ &= \sum_{M_C} \sum_{M'_C} C_1 \odot C_2 \end{aligned}$$

As a result, the Gram Jacobian $\mathbf{J}\mathbf{J}^\top$ for any layer can be obtained by a reduction on the Hadamard product of two small covariance tensors. In the following Corollary we state the conditions such that Theorem 2 improves the performance in practice by reducing the computation complexity.

Corollary 2 Suppose we show the size of common dimensions, independent dimensions and free dimensions by $N_C = \prod_{m_C \in M_C} m_C$, $N_I = \prod_{m_I \in M_I} m_I$ and N_v . Then Theorem 2 reduces the complexity of Gram matrix computation from $O(m^2 N_I N_v + m N_I N_v N_C)$ to $O(m^2 N_C^2 (N_I + N_v))$.

Remark 1 Theorem 2 applies to a wide range of layers in deep neural networks such as fully connected, convolution, and group convolution. It can also be applied to layers with nonlinear transformation as long as the non-linearity only applies to the input data such as layer normalization.

A.3 Proofs of Section 4

A.3.1 Convergence Analysis of TENGraD

In this section, we provide the proof for Theorem 1. If Assumption 2 holds, we have $\|\hat{\mathbf{J}}(\boldsymbol{\theta}) - \hat{\mathbf{J}}(0)\|_2 \leq \frac{C}{3} \lambda_0^{\frac{1}{2}}$. This result can help bound the minimum eigenvalue of the Gram Jacobian at each iteration, stated in the following Lemma.

Lemma 2 If $\|\boldsymbol{\theta}(k) - \boldsymbol{\theta}(0)\|_2 \leq 3\lambda_0^{-\frac{1}{2}} \|y - u(0)\|_2$, then we have $\lambda_{\min}(\hat{\mathbf{G}}(k)) \geq \frac{4}{9} \lambda_0$.

Proof of Lemma 2. Based on the inequality $\sigma_{\min}(A + B) \geq \sigma_{\min}(A) - \sigma_{\max}(B)$ and based on the fact that $\|\hat{\mathbf{J}}(\boldsymbol{\theta}) - \hat{\mathbf{J}}(0)\|_2 \leq \frac{C}{3} \lambda_0^{\frac{1}{2}}$, we have:

$$\begin{aligned} \sigma_{\min}(\hat{\mathbf{J}}(k)) &\geq \sigma_{\min}(\hat{\mathbf{J}}(0)) - \|\hat{\mathbf{J}}(k) - \hat{\mathbf{J}}(0)\|_2 \\ &\geq \lambda_0^{\frac{1}{2}} - \frac{1}{3} \lambda_0^{\frac{1}{2}} = \frac{2}{3} \lambda_0^{\frac{1}{2}} \Rightarrow \lambda_{\min}(\hat{\mathbf{G}}(k)) \geq \frac{4}{9} \lambda_0 \end{aligned}$$

We can now prove the linear convergence rate in Theorem 1.

Proof of Theorem 1. We prove Theorem 1 by induction. Assume $\|\mathbf{u}(k) - \mathbf{y}\|_2^2 \leq (1 - \eta)^k \|\mathbf{u}(0) - \mathbf{y}\|_2^2$. We can see that $\mathbf{J}^\top(k) = \hat{\mathbf{J}}^\top(k)\mathbf{T}$ with $\mathbf{T} \in \mathbb{R}^{Ln \times n}$ and $\mathbf{T} = [I_n, \dots, I_n]^\top$ where I_n is the identity matrix of dimension n .

$$\begin{aligned}
 \mathbf{u}(k+1) - \mathbf{u}(k) &= \mathbf{u}(\boldsymbol{\theta}(k) - \frac{\eta}{n} (\hat{\mathbf{F}}(k) + \alpha I)^{-1} \mathbf{J}(k)^\top (\mathbf{u}(k) - \mathbf{y})) - \mathbf{u}(\boldsymbol{\theta}(k)) \\
 &= - \int_{s=0}^1 \left\langle \frac{\partial \mathbf{u}(\boldsymbol{\theta}(s))}{\partial \boldsymbol{\theta}^\top}, \frac{\eta}{n} (\hat{\mathbf{F}}(k) + \alpha I)^{-1} \mathbf{J}(k)^\top (\mathbf{u}(k) - \mathbf{y}) \right\rangle ds \\
 &= - \underbrace{\int_{s=0}^1 \left\langle \frac{\partial \mathbf{u}(\boldsymbol{\theta}(k))}{\partial \boldsymbol{\theta}^\top}, \frac{\eta}{n} (\hat{\mathbf{F}}(k) + \alpha I)^{-1} \mathbf{J}(k)^\top (\mathbf{u}(k) - \mathbf{y}) \right\rangle ds}_{\textcircled{1}} \\
 &\quad + \underbrace{\int_{s=0}^1 \left\langle \frac{\partial \mathbf{u}(\boldsymbol{\theta}(k))}{\partial \boldsymbol{\theta}^\top} - \frac{\partial \mathbf{u}(\boldsymbol{\theta}(s))}{\partial \boldsymbol{\theta}^\top}, \frac{\eta}{n} (\hat{\mathbf{F}}(k) + \alpha I)^{-1} \mathbf{J}(k)^\top (\mathbf{u}(k) - \mathbf{y}) \right\rangle ds}_{\textcircled{2}}
 \end{aligned}$$

where $\boldsymbol{\theta}(s) = \boldsymbol{\theta}(k) - \frac{s\eta}{n} (\hat{\mathbf{F}}(k) + \alpha I)^{-1} \mathbf{J}(k)^\top (\mathbf{u}(k) - \mathbf{y})$. Now, we bound each term separately:

$$\begin{aligned}
 \textcircled{1} &= -\frac{\eta}{n} \mathbf{J}(k) (\hat{\mathbf{F}}(k) + \alpha I)^{-1} \mathbf{J}(k)^\top (\mathbf{u}(k) - \mathbf{y}) \tag{18} \\
 \|\textcircled{2}\|_2 &\leq \frac{\eta}{n} \left\| \int_{s=0}^1 \mathbf{J}(\boldsymbol{\theta}(s)) - \mathbf{J}(\boldsymbol{\theta}(k)) ds \right\|_2 \left\| (\hat{\mathbf{F}}(k) + \alpha I)^{-1} \mathbf{J}(k)^\top (\mathbf{u}(k) - \mathbf{y}) \right\|_2 \\
 &\stackrel{(i)}{\leq} \frac{\eta 2C}{3n} \lambda_0^{\frac{1}{2}} \left\| \left(\frac{1}{n} \hat{\mathbf{J}}^\top \hat{\mathbf{J}} + \alpha I \right)^{-1} \hat{\mathbf{J}}^\top \mathbf{T} (\mathbf{u}(k) - \mathbf{y}) \right\|_2 \\
 &\stackrel{(ii)}{\leq} \frac{\eta 2C}{3} \lambda_0^{\frac{1}{2}} \frac{\lambda_{\min}(\hat{\mathbf{G}}(k))^{\frac{1}{2}}}{\lambda_{\min}(\hat{\mathbf{G}}(k)) + n\alpha} \|\mathbf{T}(\mathbf{u}(k) - \mathbf{y})\|_2 \\
 &\stackrel{(iii)}{\leq} \frac{\eta C \lambda_0 \sqrt{L}}{\lambda_0 + \frac{9}{4}n\alpha} \|\mathbf{u}(k) - \mathbf{y}\|_2 \tag{19}
 \end{aligned}$$

We use Assumption 2 for the second inequality (i) which implies:

$$\begin{aligned}
 \left\| \int_{s=0}^1 \mathbf{J}(\boldsymbol{\theta}(s)) - \mathbf{J}(\boldsymbol{\theta}(k)) ds \right\|_2 &\leq \|\mathbf{J}(\boldsymbol{\theta}(k)) - \mathbf{J}(\boldsymbol{\theta}(0))\|_2 + \|\mathbf{J}(\boldsymbol{\theta}(k+1)) - \mathbf{J}(\boldsymbol{\theta}(0))\|_2 \\
 &\leq \frac{2C}{3} \lambda_0^{\frac{1}{2}}.
 \end{aligned}$$

The inequality (ii) follows from Lemma 2 and in the last inequality (iii) we have used the fact that $\|\mathbf{T}(\mathbf{u}(k) - \mathbf{y})\|_2 = \sqrt{L} \|(\mathbf{u}(k) - \mathbf{y})\|_2$. Finally, we are ready to prove the convergence:

$$\begin{aligned}
 \|\mathbf{u}(k+1) - \mathbf{y}\|_2^2 &\leq \|\mathbf{u}(k) - \mathbf{y}\|_2^2 - 2(\mathbf{y} - \mathbf{u}(k))^\top (\mathbf{u}(k+1) - \mathbf{u}(k)) + \|\mathbf{u}(k+1) - \mathbf{u}(k)\|_2^2 \\
 &\leq \|\mathbf{u}(k) - \mathbf{y}\|_2^2 - \frac{2\eta}{n} \underbrace{(\mathbf{y} - \mathbf{u}(k))^\top \mathbf{J}(k) \left(\hat{\mathbf{F}}(k) + \alpha I \right)^{-1} \mathbf{J}(k)^\top (\mathbf{y} - \mathbf{u}(k))}_{\text{(A)}} \\
 &\quad + \frac{2\eta C \lambda_0 \sqrt{L}}{\lambda_0 + \frac{9}{4}n\alpha} \|(\mathbf{u}(k) - \mathbf{y})\|_2^2 + \underbrace{\|\mathbf{u}(k+1) - \mathbf{u}(k)\|_2^2}_{\text{(B)}} \\
 &\leq \|\mathbf{u}(k) - \mathbf{y}\|_2^2 - \frac{2\eta L \lambda_0}{\lambda_0 + \frac{9}{4}n\alpha} \|\mathbf{u}(k) - \mathbf{y}\|_2^2 + \frac{2\eta C \lambda_0 \sqrt{L}}{\lambda_0 + \frac{9}{4}n\alpha} \|(\mathbf{u}(k) - \mathbf{y})\|_2^2 \\
 &\quad + \eta^2 \left(L + \frac{C \lambda_0 \sqrt{L}}{\lambda_0 + \frac{9}{4}n\alpha} \right)^2 \|(\mathbf{u}(k) - \mathbf{y})\|_2^2 \\
 &\leq (1 - \eta) \|(\mathbf{u}(k) - \mathbf{y})\|_2^2,
 \end{aligned}$$

where in the last inequality we use the assumption that $\eta < \frac{2L\gamma - 1 - 2C\sqrt{L}\gamma}{(L + C\sqrt{L}\gamma)^2}$ where $\gamma = \frac{\lambda_0}{\lambda_0 + \frac{9}{4}n\alpha}$. Part (A) follows from Lemma 2:

$$\text{(A)} \leq nL \|\mathbf{u}(k) - \mathbf{y}\|_2^2 \frac{\lambda_{\min} \hat{\mathbf{G}}(k)}{\lambda_{\min} \hat{\mathbf{G}}(k) + n\alpha} \leq \frac{nL\lambda_0}{\lambda_0 + \frac{9}{4}n\alpha} \|\mathbf{u}(k) - \mathbf{y}\|_2^2,$$

Part (B), on the other hand, is implied by Equation (18) and Inequality (19).

A.3.2 Bounding λ_0

The results [25] are not directly applicable to our setting as we work with block-diagonal matrices. In the following, we introduce the assumptions previously made in [25] and adapt their proofs to our setting with some modifications for providing a bound on the smallest eigenvalue of the Gram matrix.

Assumption 3 (Scaling) *The distribution of the data P_X satisfies the conditions: $\mathbb{E}_{P_X} [\|x\|_2] = \Theta(\sqrt{d})$, $\mathbb{E}_{P_X} [\|x\|_2^2] = \Theta(d)$, and $\mathbb{E}_{P_X} [\|x - \mathbb{E}_{P_X}[x]\|_2^2] = \Omega(d)$.*

Assumption 4 (Lipschitz Concentration) *For every Lipschitz continuous function f with Lipschitz constant $\|f\|_{Lip}$, the random variable $f(x)$ is Sub-Gaussian. That is there exists an absolute constant $c > 0$ such that for all $t > 0$, we have $\mathbb{P}\{|f(x) - \mathbb{E}_{P_X}[f(x)]| > t\} \leq 2 \exp\left\{-\frac{ct^2}{\|f\|_{Lip}^2}\right\}$.*

Assumption 4 is satisfied for the family of distributions satisfying log Sobolev inequality with a dimension independent constant [25]. Under these assumptions on P_X , the authors of [25] have provided tight bounds on the smallest and largest eigenvalues of empirical Neural Tangent Kernel $\bar{K}^{(L)} := \sum_{l=1}^L \mathbf{J}_l(k) \mathbf{J}_l(k)^\top$ by studying the spectrum of $\mathbf{J}_l(k) \mathbf{J}_l(k)^\top$ for each layer l . Therefore, their result translates to the spectrum of $\hat{\mathbf{J}}(k) \hat{\mathbf{J}}(k)^\top$ which is given by eigenvalues of $\mathbf{J}_l(k) \mathbf{J}_l(k)^\top$. We present the lower bound on λ_0 suggested by [25, Theorem 4.1] at Lemma 3 below and provide its derivation for the sake of completeness.

Lemma 3 *Consider a L -layer ReLU network with single output. Let weights of the network at each layer $l \in [L]$ be $W_l \in \mathbb{R}^{d_{l-1} \times d_l}$ and initialized as $(W_l)_{ij} \sim \mathcal{N}(0, \beta_l^2)$ for $l \in [L]$. Assume that data points $\{x_i, y_i\}$ are i.i.d. and drawn from a distribution P_X which satisfies the Assumptions 3 and 4. Fix any $\delta > 0$, and any even integer $r \geq 2$. Let $\mu_r(\sigma)$ be r -th Hermite coefficient of ReLU activation function σ given as*

$$\mu_r(\sigma) = \frac{1}{\sqrt{2\pi}} (-1)^{\frac{r-2}{2}} \frac{(r-3)}{\sqrt{r!}}.$$

Suppose the number of neurons at each layer $l \in [L-1]$ satisfies the conditions

$$d_l = \Omega\left(N \log(N) \log\left(\frac{N}{\delta}\right)\right) \quad \& \quad \prod_{j=1}^{l-2} \log(d_j) = o\left(\min_{j \in [0, l-1]} d_j\right),$$

then the following inequality holds for all $k \geq 0$

$$\lambda_{\min}(\hat{\mathbf{J}}(k)\hat{\mathbf{J}}(k)^\top) \geq \min_{l \in [L]} \left\{ \mu_r(\sigma)^2 \Omega \left(d \prod_{j=1}^{L-1} d_j \prod_{j=1, j \neq l}^L \beta_j^2 \right), \lambda_{\min}(XX^\top) \Omega \left(\prod_{l=1}^{L-1} d_l \prod_{l=2}^L \beta_l^2 \right) \right\},$$

with probability at least

$$1 - \delta - N^2 \exp \left(-\Omega \left(\frac{\min_{l' \in [0, L-1]} n_{l'}}{N^{2/(r-0.1)} \prod_{l'=1}^{l'-2} \log(d_{l'})} \right) \right) - N \sum_{l'=1}^{l-1} \exp(-\Omega(d_{l'})) - N \exp(-\Omega(d)).$$

Proof of Lemma 3 In our analysis, we consider a L -layer ReLU network whose weights and biases are given by matrices $W_l \in \mathbb{R}^{d_{l-1} \times d_l}$ and each feature map $f_l : \mathbb{R}^d \rightarrow \mathbb{R}^{d_l}$ is defined as

$$f_l(x) = \begin{cases} x, & \text{if } l = 0 \\ \sigma(W_l^\top f_{l-1}), & \text{if } l \in [L-1] \\ W_L^\top f_{L-1}. & \text{if } l = L \end{cases}$$

where the Fisher-block matrix is written as $\hat{\mathbf{F}}(\mathbf{W}(k)) = \hat{\mathbf{J}}(k)\hat{\mathbf{J}}(k)^\top$ with

$$\hat{\mathbf{J}}(k) = \begin{bmatrix} \mathbf{J}_1(k) & 0 & \dots & 0 \\ 0 & \mathbf{J}_2(k) & \dots & 0 \\ \vdots & \ddots & & \vdots \\ 0 & \dots & 0 & \mathbf{J}_L(k) \end{bmatrix}$$

and each $\mathbf{J}_l(k)$ is the Jacobian of the network w.r.t the parameters in the layer l , i.e. $\mathbf{J}_l(k) = \frac{\partial \mathbf{f}(\mathbf{W}(k))}{\partial \text{vec}(W_l)}$. The result follows from [25, Theorem 4.1], but for completeness we provide it here. Let $\mathcal{O}_{l,j}(x)$ be the pre-activation neuron, $\sigma(\cdot)$ be the ReLU function, and $\Sigma_l(x) = \text{Diag} \left(\sigma'(\mathcal{O}_{l,j}(x)) \right)_{j=1}^{d_l} \in \mathbb{R}^{d_l \times d_l}$. We can write the following equation for each of the layer l :

$$\left(\frac{\partial F_L}{\partial \text{vec}(W_l)} \right) \left(\frac{\partial F_L}{\partial \text{vec}(W_l)} \right)^\top = \mathbf{f}_{l-1} \mathbf{f}_{l-1}^\top \circ B_l B_l^\top$$

where $\mathbf{f}_l = \left[\frac{\partial f_l(\mathbf{W}; x_1)}{\partial \text{vec}(W_l)}, \dots, \frac{\partial f_l(\mathbf{W}; x_n)}{\partial \text{vec}(W_l)} \right]^\top$ and $B_l \in \mathbb{R}^{N \times N}$ is a matrix whose i -th row is given as

$$[B_l]_{i:} = \begin{cases} \Sigma_l(x_i) \left(\prod_{l'=l+1}^{L-1} W_{l'} \Sigma_{l'}(x_i) \right) W_L, & l \in [0, L-2] \\ \Sigma_{L-1}(x_i) W_L, & l = L-1 \\ \frac{1}{\sqrt{N}} \mathbf{1}_N, & l = L \end{cases}$$

The result relies on the inequality

$$\lambda_{\min}(F_{l-1} F_{l-1}^\top \circ B_l B_l^\top) \geq \lambda_{\min}(F_{l-1} F_{l-1}^\top) \min_{i \in \{1, \dots, N\}} \|[B_l]_{i:}\|_2^2.$$

The Lemma 4.3 given at [25] yields that for any layer $l \in [1, \dots, L-2]$ and $x \sim P_X$ the following holds

$$\left\| \Sigma_{l+1}(x) \left(\prod_{l'=l+2}^{L-1} W_{l'} \Sigma_{l'}(x) W_L \right) \right\|_2^2 = \Theta \left(\beta_L^2 d_{l+1} \prod_{l'=l+2}^{L-1} d_{l'} \beta_{l'}^2 \right)$$

w.p. at least $1 - \sum_{l=1}^{L-1} \exp\{-\Omega(d_l)\} - \exp(-\Omega(d))$ assuming that the product term $\prod_{l'=l+2}^{L-1} (\cdot)$ is inactive for $l = L-2$. The Theorem 5.1 at [25] provides the lower bound on $\lambda_{\min}(F_l F_l^\top)$ which depends on $\mu_r(\sigma)$ in addition to problem parameters d, d_1, \dots, d_L . If we fix $l \in \{1, \dots, L-1\}$ and any integer $r > 0$, then for $\delta > 0$ and the d_l satisfying $d_l = \Omega \left(N \log(N) \log\left(\frac{N}{\delta}\right) \right)$ and $\prod_{l'=1}^{l-2} \log(d_{l'}) = o(\min_{l' \in [0, l-1]} d_{l'})$, the smallest singular value of F_l satisfies the inequality

$$\sigma_{\min}(F_l)^2 \geq \mu_r(\sigma)^2 \Omega \left(d \prod_{l'=1}^l d_{l'} \beta_{l'} \right)$$

w.p. at least

$$1 - \delta - N^2 \exp \left(-\Omega \left(\frac{\min_{l' \in [0, l-1]} n_{l'}}{N^{2/(r-0.1)} \prod_{l'=1}^{l'-2} \log(d_{l'})} \right) \right) - N \sum_{l'=1}^{l-1} \exp(-\Omega(d_{l'})) - N \exp(-\Omega(d)).$$

A.4 Experiments

This section provides additional details on experiments and extra results. First, we provide details of the DNN architectures used in the experiments and then the training process and finally, we show additional results.

A.4.1 Experimental Setup

DNN Architectures For the Fashion-MNIST benchmark, we use a model with three convolutional layers and one fully connected layer. The first convolutional layer has one input channel and 128 output channels. The second and third layers have 128 in both input and output channels. The padding and stride are set to 1 and the kernel size is 3. The fully connected layer has an input of $9^2 \times 128$ and output of size 500. All the layers are followed by ReLU activation functions. Finally, there is a fully connected layer with 10 outputs and no activation. For CIFAR-10 and CIFAR-100 we use the DenseNet [28], WideResNet [29] and MobileNetV2 [30] architectures. For WideResNet model, we use depth=28 and a widen factor of 4. For DenseNet we set depth to 19 and choose a growth rate of 100. For MobileNetV2 we use the default model.

Training Process In all of the experiments, we use a batch size of 128 samples which is widely used in practice. We also apply momentum to all optimization methods since, from observation, it improves the training time and accuracy for all methods. To avoid over-fitting, we apply a standard weight decay where the weight decay parameter is tuned. For Fashion-MNIST we set the number of epochs to 10 and for CIFAR-10 and CIFAR-100, we use 60 epochs. For NGD methods we use a frequency of inversion of 100 to amortize the cost of updates. For EKFac we set the scaling frequency to 20.

Learning rate strategy. For Fashion-MNIST we fix the learning rate during training. For CIFAR-10, a decaying learning rate strategy is used to achieve state-of-the-art accuracy which is a typical in practice. We decay the learning rate by half after every 10 epochs. For CIFAR-100, we decay the learning rate by 0.1 after epochs 30 and 45.

Tuning parameters. We tune the parameter learning rate, weight decay, and dampening and use a grid search. The range of learning rate is $\{0.001, 0.003, 0.01, 0.03, 0.1, 0.3\}$. The range for the weight decay is $\{0.001, 0.003, 0.01, 0.3, 0.1, 0.3\}$. The range of damping parameter is $\{0.001, 0.003, 0.01, 0.03, 0.1, 0.2, 0.3\}$. The momentum is set to 0.9. Table 4, Table 5 and Table 3 provide the tuned values for the parameters of each experiment.

Table 3: Tuned parameters (learning rate, weight decay and damping) for the Fashion-MNIST experiments.

	TENGrAD	KFAC	EKFAC	KBFGS	SGD
3CIF	0.003, 0.001, 0.1	0.003, 0.001, 0.1	0.001, 0.003, 0.03	0.03, 0.01, 0.01	0.03, 0.001

Table 4: Tuned parameters (learning rate, weight decay and damping) for the CIFAR-10 experiments.

	TENGrAD	KFAC	EKFAC	KBFGS	SGD
WideResNet	0.03, 0.003, 0.1	0.03, 0.003, 0.03	0.01, 0.003, 0.03	0.03, 0.003, 0.03	0.01, 0.003
DenseNet	0.1, 0.003, 0.2	0.01, 0.003, 0.03	0.01, 0.003, 0.01	0.01, 0.003, 0.01	0.03, 0.003
MobileNetV2	0.01, 0.01, 0.2	0.01, 0.003, 0.1	0.01, 0.003, 0.1	0.01, 0.03, 0.03	0.01, 0.003

Table 5: Tuned parameters (learning rate, weight decay and damping) for the CIFAR-100 experiments.

	TENGrAD	KFAC	EKFAC	KBFGS	SGD
WideResNet	0.01, 0.03, 0.3	0.003, 0.01, 0.03	0.003, 0.01, 0.03	0.003, 0.01, 0.01	0.01, 0.003
DenseNet	0.1, 0.003, 0.1	0.01, 0.003, 0.03	0.01, 0.003, 0.03	0.01, 0.003, 0.03	0.01, 0.003
MobileNetV2	0.01, 0.01, 0.3	0.01, 0.003, 0.03	0.01, 0.003, 0.03	0.03, 0.01, 0.03	0.01, 0.003

A.4.2 Structure of Block Inverses

In order to compare the quality of FIM approximation, we compare the diagonal block approximations in TENGrAD and KFAC with the exact NGD method. The structure for the third convolution layer and the fully connected layer in the 3CIF model are shown in Figure 7 and Figure 8. TENGrAD keeps the block structure of the Fisher inverse similar to that of exact NGD while KFAC has a different pattern due to its specific Kronecker structure. Moreover, KFAC still approximates the block inverse with a diagonally dominant matrix in the third convolution layer.

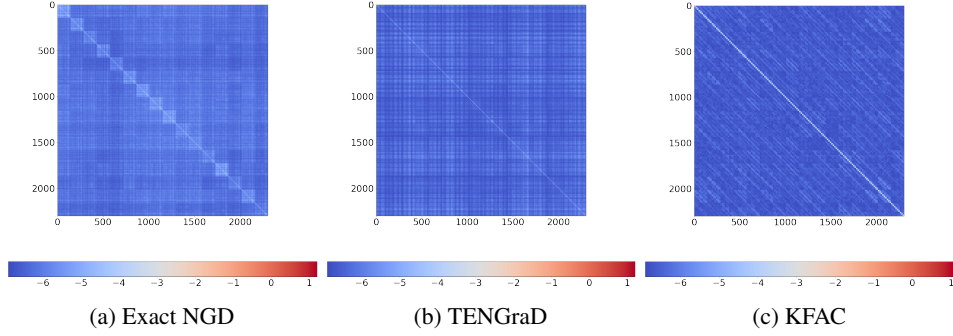


Figure 7: Structure of block inverses for the third convolution layer in 3C1F with Fashion-MNIST.

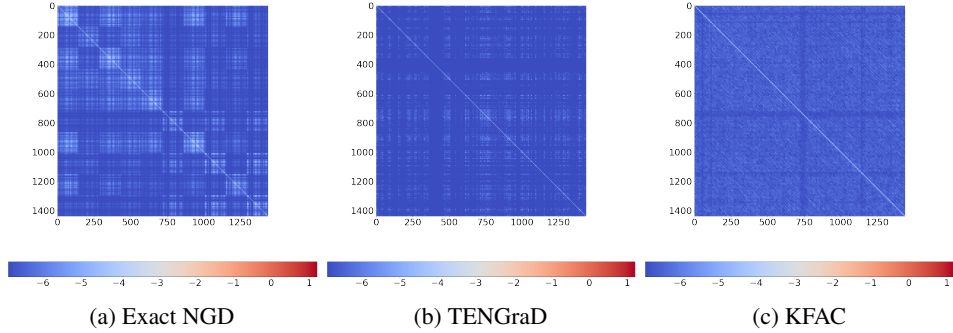


Figure 8: Structure of block inverses for the fully connected layer in 3C1F with Fashion-MNIST.

A.4.3 Sensitivity to Hyperparameters

To demonstrate the robustness, we examine the train and test accuracy under various hyperparameter (HP) settings and show TENGrAD is stable under a wide range for the HPs. The train and test accuracy for the Fashion-MNIST benchmark under different HP settings is shown in Figure 9 and Figure 10. Also, we observe that a larger damping parameter allows for larger step sizes. TENGrAD allows for a wide range of HP to be used with almost no loss of accuracy on both train and test data.

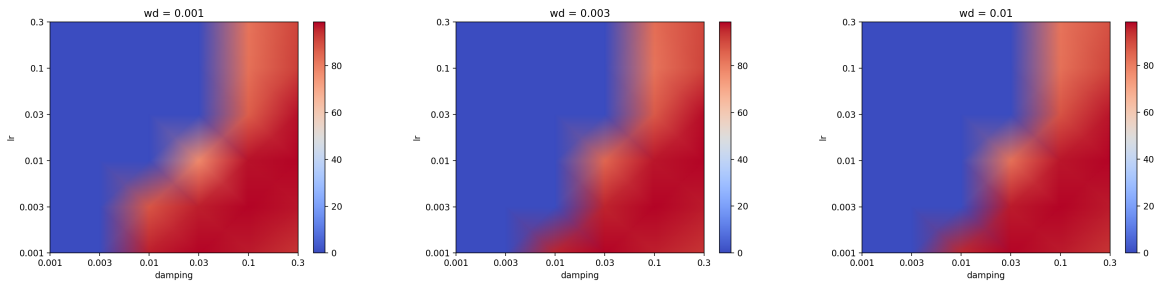


Figure 9: The train accuracy for the Fashion-MNIST benchmark under various hyperparameter settings for the test samples.

A.5 Error Bar Plots

The error bars for the Fashion-MNIST benchmark are shown in Figure 11. TENGrAD outperforms both SGD and other NGD methods in time and accuracy. The error bar plots for five different runs of the CIFAR-10 benchmark are shown in Figure 12 and Figure 13. TENGrAD outperforms other NGD methods in time and accuracy for both train and test. In Figure 12b the train accuracy of KBFGRS appears to be better than that of TENGrAD but the corresponding test accuracy in Figure 13b shows that TENGrAD has a higher test accuracy and does not over-fit to data. The error bars of train and test for the CIFAR-100 benchmark are shown in Figure 14 and Figure 15. TENGrAD outperforms SGD in time and

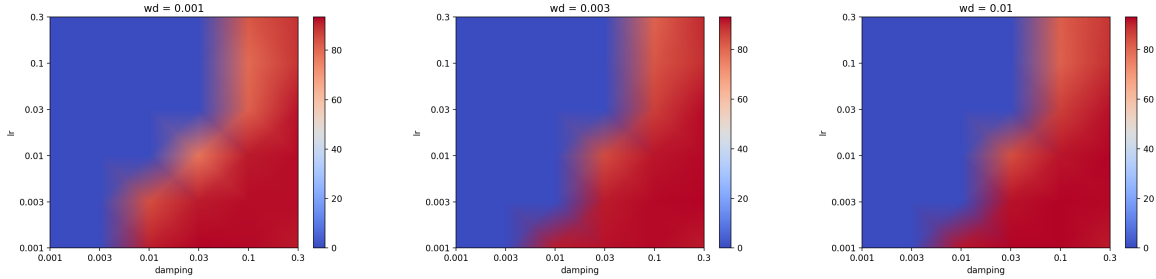


Figure 10: The test accuracy for Fashion-MNIST benchmark under various hyperparameter settings for the test samples.

accuracy in training the DenseNet model as shown in Figure 14a and achieves a better accuracy compared to all other methods as shown in Figure 15a. TENGrAD is also competitive with SGD on other benchmarks and outperforms other NGD methods.

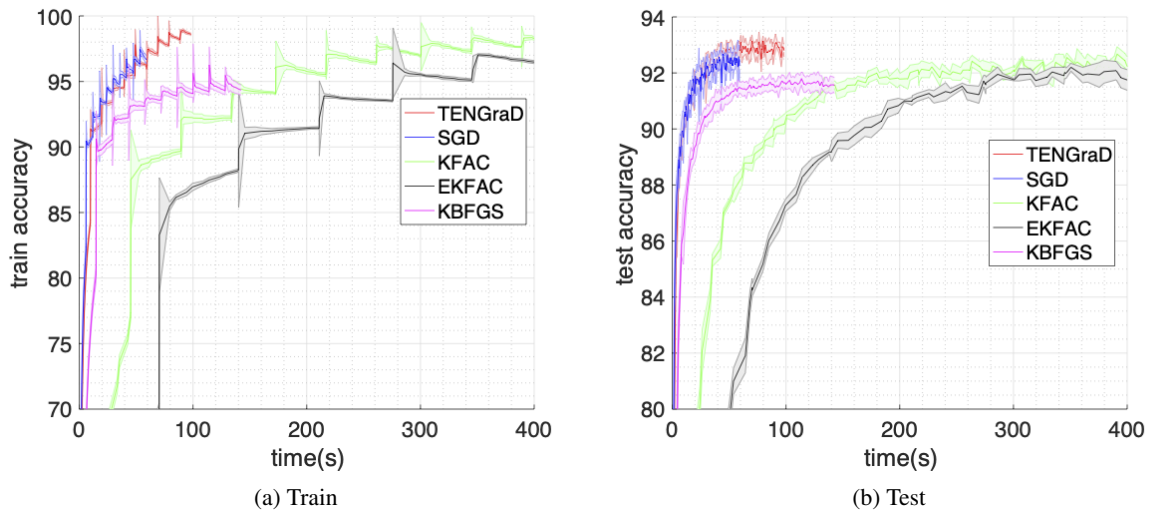


Figure 11: The error bars of train and test accuracy for Fashion-MNIST benchmark.

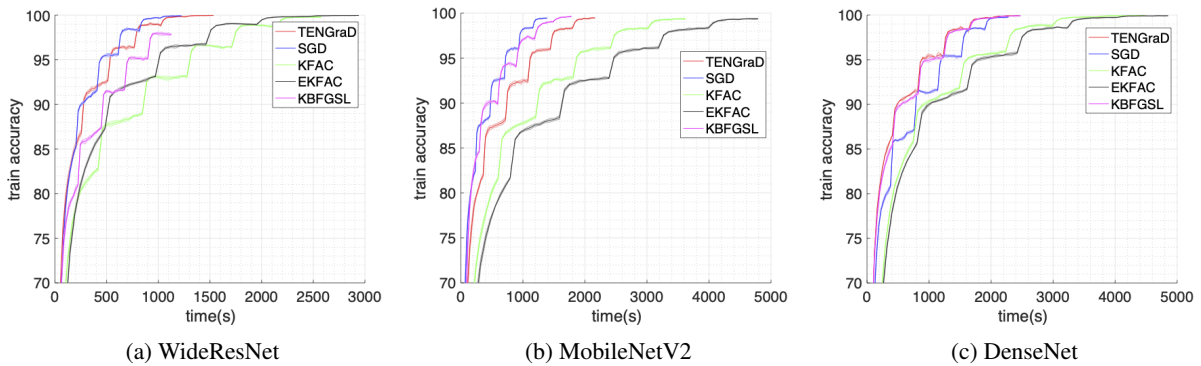


Figure 12: The error bars of train accuracy for CIFAR-10 benchmark.

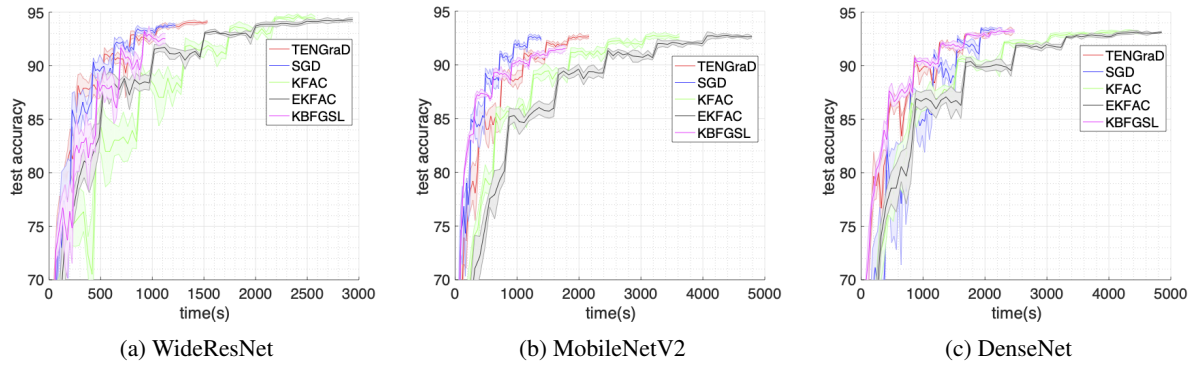


Figure 13: The error bars of test accuracy for CIFAR-10 benchmark.

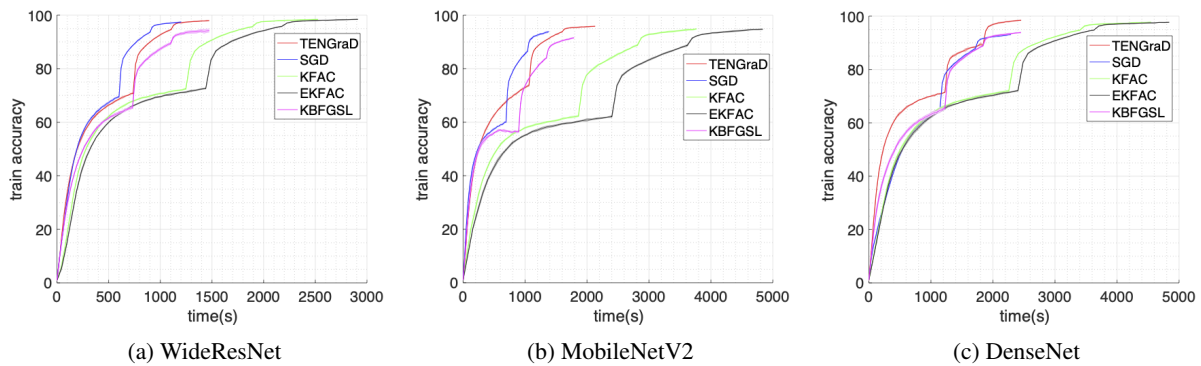


Figure 14: The error bars of train accuracy for CIFAR-100 benchmark.

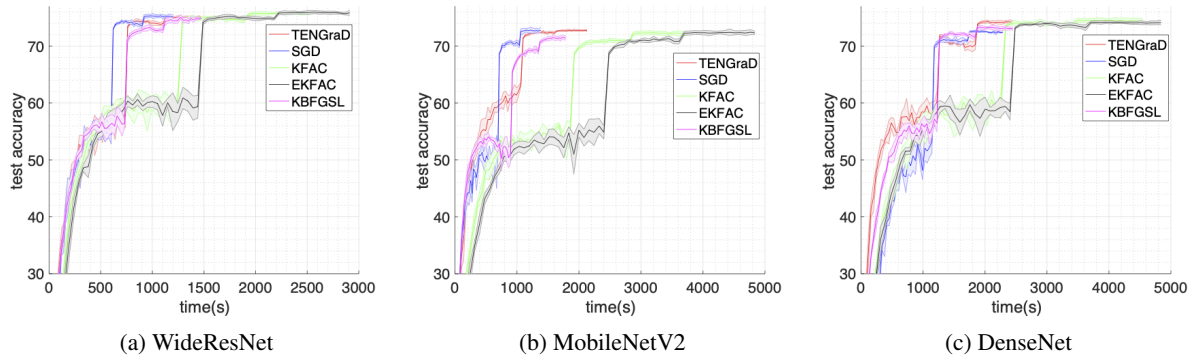


Figure 15: The error bars of test accuracy for CIFAR-100 benchmark.